*Inorg. Chem.* **2004**, *43*, 5245–5252


# High Pressure Study of $Ru_3(CO)_{12}$ by X-ray Diffraction, Raman, and Infrared Spectroscopy

**Carla Slebodnick,[†] Jing Zhao,[‡] Ross Angel,[‡] Brian E. Hanson,*[,†] Yang Song,[§] Zhenxian Liu,[§] and Russell J. Hemley[§]**

*Departments of Chemistry and GeoSciences, Virginia Tech, Blacksburg, Virginia 24061, and Geophysical Laboratory, Carnegie Institute of Washington, Broad Branch Road, Washington, D.C. 20001*

Received March 22, 2004

The single-crystal X-ray structure of $Ru_3(CO)_{12}$ is reported at 8 pressures ranging from 1 atm (0.0 GPa) to 8.14(5) GPa. Although intramolecular bonding parameters remain relatively constant, intramolecular and intermolecular nonbonding contact distances decrease by an average of 4% and 15%, respectively. At 8.14 GPa, O···O, C···O, and C···C intermolecular distances as short as 2.54(4), 2.64(6), and 3.07(4) Å, respectively, are observed, and the unit cell compresses to 75% of the ambient pressure volume. Raman and infrared spectroscopic measurements show that carbonyl stretching frequencies shift to higher wavenumber values by as much as 80 $cm^{-1}$, even though Ru–C and C–O distances stay roughly constant throughout the entire pressure range studied. Compression of the sample to above 18 GPa with laser radiation results in an irreversible transformation due to either decomposition or a total collapse of $D_{3h}$ molecular geometry accompanied by color darkening.

## Introduction

The structures of the trinuclear metal carbonyl clusters $M_3(CO)_{12}$ (M = Fe, Ru, Os) have been thoroughly studied over the last 50 years.[1−8] The structure of $Fe_3(CO)_{12}$ is reported in the Cambridge Structural Database[9,10] nine times, at temperatures ranging from 100 to 320 K.[1−4,8,11] The $Fe_3(CO)_{12}$ structure collected at 123 K is best described as a superlattice of slightly rotated structures.[8] Four structures of $Ru_3(CO)_{12}$ at temperatures ranging from ambient down to 100 K are also available.[5,7,12] These compounds are of long-standing interest because of their central role in defining some of the key concepts in the structural chemistry of metal carbonyls. For example, the fact that carbonyl positions define the vertices of polyhedra was recognized in the first complete description of the structure of $Fe_3(CO)_{12}$.[2] Also, a potential mechanism for fluxional processes in the trinuclear clusters was derived in part from the recognition of the close similarity of the $Fe_3(CO)_{12}$ and $Ru_3(CO)_{12}$ structures.[3] Specifically, the smaller icosahedral $Fe_3(CO)_{12}$ structure could momentarily open up to the larger anticuboctahedral $Ru_3(CO)_{12}$ structure thereby scrambling the carbonyl ligands. Smaller metal clusters, such as $Fe_3$, fit inside the compact icosahedral arrangement of carbonyl groups while larger clusters, such as $Ru_3$ and $Os_3$, require the larger cavity provided by the anticuboctahedral cluster. Huckel calculations suggest the bridging structure is feasible for triiron dodecacarbonyl and not for the ruthenium and osmium compounds due to the fact that there is less repulsion between iron atoms than in the heavier metals. This allows the iron atoms to get sufficiently close to allow the bridging carbonyls. Further, it was estimated that the all terminal structure

* To whom correspondence should be addressed. E-mail: hanson@vt.edu.
[†] Department of Chemistry, Virginia Tech.
[‡] Department of GeoSciences, Virginia Tech.
[§] Carnegie Institute of Washington.

(1) Dahl, L. F.; Rundle, R. E. *J. Chem. Phys.* **1957**, *26*, 1751−1752.
(2) Wei, C. H.; Dahl, L. F. *J. Am. Chem. Soc.* **1969**, *91*, 1351−1361.
(3) Cotton, F. A.; Troup, J. M. *J. Am. Chem. Soc.* **1974**, *96*, 4155−4159.
(4) Braga, D.; Farrugia, L.; Grepioni, F.; Johnson, B. F. G. *J. Organomet. Chem.* **1994**, *464* (2), C39−C41.
(5) Braga, D.; Grepioni, F.; Tedesco, E.; Dyson, P. J.; Martin, C. M.; Johnson, B. F. G. *Transition Met. Chem.* **1995**, *20* (6), 615−624.
(6) Braga, D.; Farrugia, L.; Gillon, A. L.; Grepioni, F.; Tedesco, E. *Organometallics* **1996**, *15* (22), 4684−4686.
(7) Mason, R.; Rae, A. I. M. *J. Chem. Soc. A* **1968**, 778−779.
(8) Farrugia, L. J.; Gillon, A. L.; Braga, D.; Grepioni, F. *Organometallics* **1999**, *18* (24), 5022−5033.
(9) Allan, F. H. *Acta Crystallogr.* **2002**, *B58*, 380−388.
(10) Bruno, I. J.; Cole, J. C.; Edgington, P. R.; Kessler, M.; Macrae, C. F.; McCabe, P.; Pearson, J.; Taylor, R. *Acta Crystallogr.* **2002**, *B58*, 389−397.
(11) Braga, D.; Grepioni, F.; Farrugia, L. J.; Johnson, B. F. G. *J. Chem. Soc., Dalton Trans.* **1994**, 2911−2918.
(12) Churchill, M. R.; Hollander, F. J.; Hutchinson, J. P. *Inorg. Chem.* **1977**, *16*, 2655−2659.

10.1021/ic049617y CCC: $27.50 
Published on Web 07/21/2004

for triruthenium dodecacaronyl is 19 kJ mol$^{-1}$ more stable than a ruthenium carbonyl structure with two bridging carbonyls.[13] Additionally, it was observed in $Fe_3(CO)_{12}$ that metal carbonyl clusters can be fluxional in the solid state,[14,15] and that the disorder observed in the X-ray structures of $Fe_{3-x}Ru_x(CO)_{12}$ is dynamic.[6,8]

High-pressure X-ray diffraction data are collected by suspending the sample in a hydrostatic fluid encased within a diamond anvil cell (DAC).[16] The diamond anvil is used simultaneously to exert pressure and to provide a spectroscopic window to the material undergoing compression. Pressures in excess of 100 GPa ($10^6$ atm) can be achieved with an appropriately designed cell. The ability to access such extreme pressures allows several fundamental issues in chemistry to be investigated. For example, one can determine volumes of activation along a reaction coordinate or study pressure-induced phase changes in materials.[17−19] Specially designed DACs for single-crystal X-ray work allow structures to be determined at high pressure. Several small molecule organic compounds have been studied by X-ray diffraction at high pressure.[20]

High-pressure studies of molecular inorganic or organometallic compounds are less common. A complete structural determination of bis(dimethylglyoxime)platinum(II) at high pressure revealed that the intermolecular Pt−Pt separation[21] decreases from 3.259 Å at atmospheric pressure to 2.975 Å at 3.84 GPa and to 2.84 Å at 10 GPa.[18] This finding correlated well with the observed increase in conductivity with increased pressure; as the Pt−Pt separation decreases, the material goes through insulator to metal to insulator transitions.[18]

High-pressure Raman spectroscopic data for several metal carbonyls have also been reported. The Raman spectra of $Mn_2(CO)_{10}$ and $Re_2(CO)_{10}$ suggest a possible phase change at 5−8 kbar pressure, possibly from the staggered $D_{4d}$ structure to an eclipsed $D_{4h}$ structure.[22]

Against this background, we hypothesized that it might be possible to transform the larger volume $Ru_3(CO)_{12}$ and $Os_3(CO)_{12}$ structures to the smaller volume $Fe_3(CO)_{12}$ type structure by applying extreme pressures. The extreme pressures that can be achieved in a diamond anvil cell should far exceed the apparent energy difference between the anticuboctahedral structure and the icosahedral structure of ruthenium carbonyl.[13] Thus, we report here the single-crystal X-ray structure of $Ru_3(CO)_{12}$ at pressures up to 8.14 GPa and related Raman and infrared spectroscopy studies up to 18 GPa. Although the clusters do not adopt the smaller volume $Fe_3(CO)_{12}$ structure at high pressure and there is no evidence for a phase change between 1 atm and 10 GPa, the effects of the high pressure on unit cell volume, molecular packing, and vibrational spectroscopy are striking.

## Experimental Section

**X-ray Crystallography.** Yellow plates of $Ru_3(CO)_{12}$ (Strem Chemicals) were grown from hexanes at −15 °C. A crystal of approximate dimensions 0.22 × 0.19 × 0.030 mm$^3$ was selected for high-pressure measurement after collecting and refining a complete data set in air to confirm that the crystal was of suitable quality.

High-pressure diffraction data were collected using an ETH diamond anvil cell (DAC)[23] with anvil culets of 600 $\mu$m diameter. A 4:1 methanol−ethanol mixture was used as the pressure-transmitting medium. The sample cavity was prepared from hard T301 steel gaskets with a starting thickness of 250 $\mu$m. The gasket was preindented to a thickness of 115 $\mu$m, and then a hole of 390 $\mu$m was drilled in the center of the indented region. The chosen crystal was loaded on the surface of an anvil together with a ruby ball approximately 10 $\mu$m in diameter. Pressure was determined by monitoring the shift of the ruby R-luminescence lines[24] with a Dilor XY 0.64 m Raman microprobe and accessory spectrometer with CCD multichannel detector. Reported pressure uncertainties are the differences between the pressure measurements performed before and after each X-ray diffraction data collection.

Intensity data were collected on a kappa geometry Oxford Diffraction Xcalibur 1 diffractometer equipped with a Mo K$\alpha$ sealed tube X-ray source (0.71073 Å), graphite monochromator, and a point detector. All accessible data with $k \leq 0$ and $2° \leq 2\theta \leq 45°$ were collected using $\omega$ scans in a constant precision mode at $\varphi = 0$ to maximize access.[25] Peak profiles were integrated by full learnt-profile fitting with the WinIntegrStp 3.3 software.[26] Reflections that were not consistent with the learnt-profile from the strong reflections were rejected at this stage. Corrections for absorption effects of the DAC (i.e., Be plates, diamond anvils, shadowing by the gasket) and the sample were made using the ABSORB program.[27,28]

Starting atomic coordinates for $Ru_3(CO)_{12}$ [12] were obtained from the Cambridge Crystallographic Data Center.[9,10] SHELXTL-PC[29] was used for structure refinements. The complete data set collected in air was refined anisotropically and was fully consistent with the literature. Crystal data for $Ru_3C_{12}O_{12}$ follow: fw, 639.33; crystal system, monoclinic; space group $P2_1/n$ (No. 14).

The DAC imposes severe restrictions on which reflections can be collected, resulting in a low data/parameter ratio. As a result, the refinement can be exceedingly sensitive to a few badly corrected intensity data. Therefore, the ambient pressure (in DAC) model was refined isotropically twice, both with restraints and without


(13) Braga, D.; Grepioni, F.; Tedesco, E.; Calhorda, M. J.; Lopes, P. E. M. *J. Chem. Soc., Dalton Trans.* **1995**, 3297−3306.
(14) Dorn, H. C.; Hanson, B. E.; Motell, E. *Inorg. Chem. Acta* **1981**, *74*, L71−L72.
(15) Hanson, B. E.; Lisic, E. C.; Petty, J. T.; Iannaccone, G. *Inorg. Chem.* **1986**, *25*, 4062−4064.
(16) Miletich, R.; Allan, D. R.; Kuhs, W. F. *Rev. Mineral.* **2000**, *41*, 455−519.
(17) Shirotani, I.; Kawamura, A.; Suzuki, K.; Utsumi, W.; Yagi, T. *Bull. Chem. Soc. Jpn.* **1991**, *64* (5), 1607−1612.
(18) Takeda, K.; Shirotani, I.; Yakushi, K. *Chem. Mater.* **2000**, *12* (4), 912−916.
(19) Shirotani, I.; Hayashi, J.; Yakushi, K.; Takeda, K.; Yokota, T.; Shimizu, K.; Amaya, K.; Nakayama, A.; Aoki, K. *Physica B* **2001**, *304* (1−4), 6−11.
(20) Katrusiak, A. *Cryst. Res. Technol.* **1991**, *26* (5), 523−531.
(21) Konno, M.; Okamoto, T.; Shirotani, I. *Acta Crystallogr., Sect. B: Struct. Sci.* **1989**, *45*, 142−147.
(22) Adams, D. M.; Hatton, P. D.; Shaw, A. C. *J. Phys.: Condens. Matter* **1991**, *3* (32), 6145−6158.
(23) Allan, D. R.; Miletich, R.; Angel, R. J. *Rev. Sci. Instrum.* **1996**, *67*, 840−842.
(24) Mao, H. K.; Xu, J.; Bell, P. M. *J. Geophys. Res.* **1986**, *91*, 4673−4676.
(25) Finger, L. W.; King, H. E. *Am. Mineral.* **1978**, *63*, 337−342.
(26) Angel, R. J. *J. Appl. Crystallogr.* **2003**, *36*, 295−300.
(27) Angel, R. J. *J. Appl. Crystallogr.*, **2004**, *37*, 486−492.
(28) Burnham, C. W. *Am. Mineral.* **1966**, *51*, 159−167.
(29) Sheldrick, G. M. *SHELXTL NT*, 6.12; Bruker Analytical X-ray Systems, Inc.: Madison, WI, 2001.

**Table 1.** Crystal Data for $Ru_3(CO)_{12}$

| | air | 0.00 GPa | 0.96 GPa | 1.80 GPa | 3.43 GPa | 4.63 GPa | 5.80 Gpa | 7.12 GPa | 8.14 GPa |
|---|---|---|---|---|---|---|---|---|---|
| $\sigma P$, GPa | | $1 \times 10^{-6}$ | 0.05 | 0.01 | 0.02 | 0.03 | 0.02 | 0.05 | 0.05 |
| $a$, Å | 8.0796(4) | 8.0847(4) | 7.8785(7) | 7.7435(4) | 7.5883(7) | 7.5090(2) | 7.4412(3) | 7.3892(3) | 7.3718(3) |
| $b$, Å | 14.794(2) | 14.798(2) | 14.354 (2) | 14.1407(8) | 13.896(2) | 13.7409(4) | 13.6282(4) | 13.5531(3) | 13.5148(4) |
| $c$, Å | 14.542 (3) | 14.559 (6) | 14.138(2) | 13.828(6) | 13.5401(5) | 13.337(2) | 13.183(2) | 13.079(2) | 13.037(3) |
| $\beta$, deg | 100.611(7) | 100.62(2) | 100.47(2) | 100.195(11) | 100.34(2) | 100.147(5) | 100.132(6) | 100.244(6) | 100.232(8) |
| $V$, Å$^3$ | 1708.4(1) | 1712.0 (6) | 1572.2(2) | 1490.4(4) | 1404.6(3) | 1354.55(5) | 1316.05(4) | 1288.93(5) | 1278.2(1) |
| $\rho$, (g/cm$^3$) | 2.486 | 2.480 | 2.701 | 2.849 | 3.023 | 3.135 | 3.227 | 3.295 | 3.323 |
| reflns collected | 4776 | 1708 | 1707 | 1626 | 1519 | 1460 | 1410 | 1384 | 1382 |
| reflns integrated | 3341 | 1080 | 790 | 719 | 705 | 1018 | 1014 | 946 | 901 |
| data | 1810 | 627 | 568 | 518 | 456 | 614 | 593 | 554 | 552 |
| data ($I > 2\sigma$) | 1802 | 623 | 565 | 514 | 453 | 579 | 558 | 513 | 506 |
| $R_{int}$ | 0.047 | 0.0745 | 0.073 | 0.043 | 0.034 | 0.036 | 0.043 | 0.037 | 0.108 |
| restraints | 0 | 24 | 24 | 24 | 24 | 24 | 24 | 24 | 24 |
| params | 244 | 113 | 113 | 113 | 113 | 113 | 113 | 113 | 113 |
| GOF | 1.14 | 1.251 | 1.34 | 1.34 | 1.32 | 1.31 | 1.28 | 1.31 | 1.31 |
| restrained GOF | | 1.226 | 1.31 | 1.31 | 1.28 | 1.28 | 1.25 | 1.28 | 1.28 |
| R1 ($I > 2\sigma$) | 0.0346 | 0.0503 | 0.0498 | 0.0507 | 0.0459 | 0.0438 | 0.0441 | 0.0453 | 0.0622 |
| R1 (all data)[a] | 0.0349 | 0.0506 | 0.0513 | 0.0511 | 0.0469 | 0.0491 | 0.0487 | 0.0548 | 0.0723 |
| wR2 (all data)[a] | 0.0972 | 0.1341 | 0.1271 | 0.1256 | 0.1121 | 0.1042 | 0.1148 | 0.1142 | 0.1445 |
| lrgst diff peak | 1.24 | 0.42 | 0.52 | 0.49 | 0.50 | 0.69 | 0.79 | 0.70 | 0.72 |
| lrgst diff hole | −0.83 | −0.53 | −0.58 | −0.50 | −0.59 | −0.66 | −1.00 | −0.68 | −0.80 |

[a] $R1 = \sum||F_o| - |F_c||/\sum|F_o|$; $wR2 = [\sum[w(F_o^2 - F_c^2)^2]/\sum[w(F_o^2)^2]\,]^{1/2}$; $w = 1/[\sigma^2(F_o^2) + (aP)^2 + bP]$, where $P = 0.333[\max(0 \text{ or } F_o^2) + 2F_c^2]$.

restraints. Both models were compared to our complete data set and the literature in order to eliminate systematic errors. The nonrestrained data set showed significant deviation in some bond lengths and angles. Therefore, in order to dampen the effect of a few outlier reflections on the refinement, the DFIX command of SHELXTL was used to restrain the average Ru−C(axial) and Ru−C(equatorial) bond lengths, and the DANG command was used to restrain the av Ru···O(axial) and Ru···O(equatorial) distances. The final refinement of all DAC data sets used these same restraints. This should ensure that trends in bond lengths and angles with pressure accurately reflect the actual behavior of the structure. Data collection and structure refinement parameters are summarized in Table 1. Tables of metrical parameters were generated using PLATON.[30] Short intermolecular contacts were determined by analyzing the intermolecular contact table output by PLATON for the 8.14 GPa dataset. The equivalent contacts at the 7 lower pressures were then identified using a combination of PLATON and the XP program within SHELXTL NT. Molecular graphics were generated using the XP program within SHELXTL NT.[29]

Infrared absorption measurements were performed at beamline U2A at the National Synchrotron Light Source of Brookhaven National Laboratory, and the optical layout of the beamline facility has been described in detail elsewhere.[31] The IR spectra were collected with a Bruker IFS 66v/S vacuum Fourier transform interferometer, Bruker IRscope II microscope equipped with HgCdTe type-A detector. In order to observe the C−O stretching vibrations in $Ru_3(CO)_{12}$, a moissanite anvil cell (MAD) was used to avoid the characteristic phonon absorption of diamond.[31b] As KBr powder is very soft and one of the best solid pressure media used for high-pressure IR studies, we use it to dilute a finely grained sample with ~30:1 ratio. A ~100-$\mu$m-diameter hole was drilled at the center of a preindented gasket, and the mixture of the KBr and $Ru_3(CO)_{12}$ powder was loaded into the gasket hole. A small ruby chip was also added to monitor pressure as described above for the X-ray experiments. The spectral resolution is 1 cm$^{-1}$ with 1024 scans for all measurements at different pressures.

Raman spectroscopy was performed at the Geophysical Laboratory as previously described.[32] The sample was finely ground, and the powder was placed into a diamond anvil cell constructed with type II diamonds. A small ruby chip was added to monitor pressure as described above for the X-ray experiments; no pressure medium was added. A Coherent 890 titanium:sapphire laser was pumped by a Coherent Innova Ar ion laser to give an excitation line of 752.12 nm for spectral measurements. The collimated laser beam was typically focused on the sample in a backscattering geometry with an estimated power of less than 15 mW. It was found that the sample readily decomposed in the laser beam and low power was required to collect data.

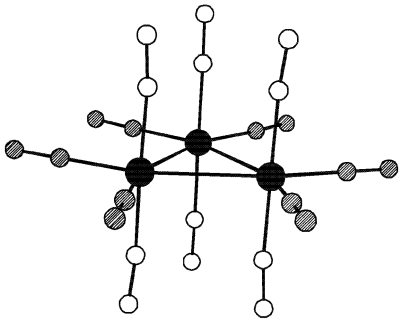

**Figure 1.** Diagram of $Ru_3(CO)_{12}$. Axial atoms are depicted as open circles and equatorial atoms as shaded circles.

## Results and Discussion

$Ru_3(CO)_{12}$ crystallizes in the space group $P2_1/n$ with one crystallographically independent molecule in the asymmetric unit. The $Ru_3(CO)_{12}$ molecule has approximate $D_{3h}$ symmetry, with each ruthenium adopting a pseudo-octahedral geometry defined by two ruthenium atoms and two carbonyls in the equatorial plane and two axial carbonyls (Figure 1). Because the diamond anvil cell limits the data-to-parameter ratio through both diminished intensity (due to absorption and scattering by the diamonds) and through restricted access to reciprocal space (due to the bulk of the DAC), a few outlier reflections can have a significant effect on the overall

(30) Spek, A. L. *J. Appl. Crystallogr.* **2003**, *36*, 7−13.
(31) (a) Liu, Z. X.; Hu, J.; Yang, H.; Mao, H. K.; Hemley, R. J. *J. Phys.: Condens. Matter* **2002**, *14*, 10641. (b) Liu, Z. X.; Mao, H. K.; Hemley, R. J. *Rev. Sci. Instrum.*, submitted.
(32) Song, Y.; Hemley, R. J.; Liu, Z. X.; Somayazulu, M.; Mao, H. K.; Herschbach, D. R. *J. Chem. Phys.* **2003**, *119*, 2232−2240.

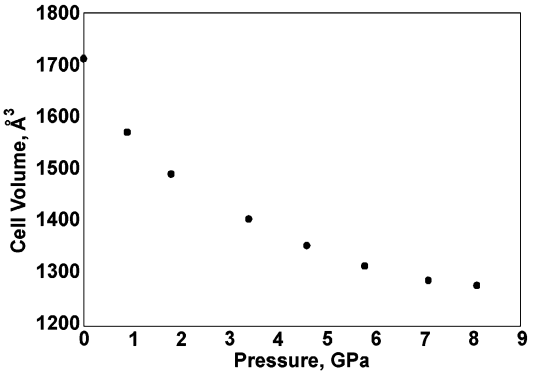


**Figure 2.** Unit cell volume as a function of pressure.

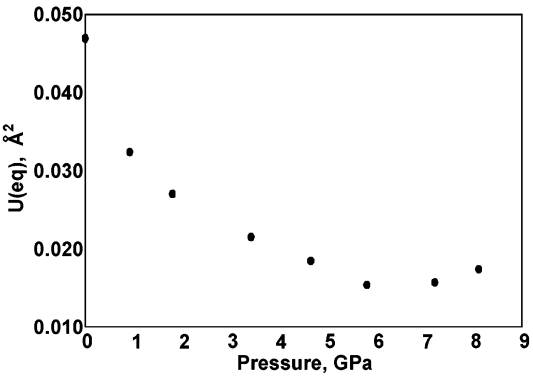


**Figure 3.** Average istotropic displacement parameters as a function of pressure.

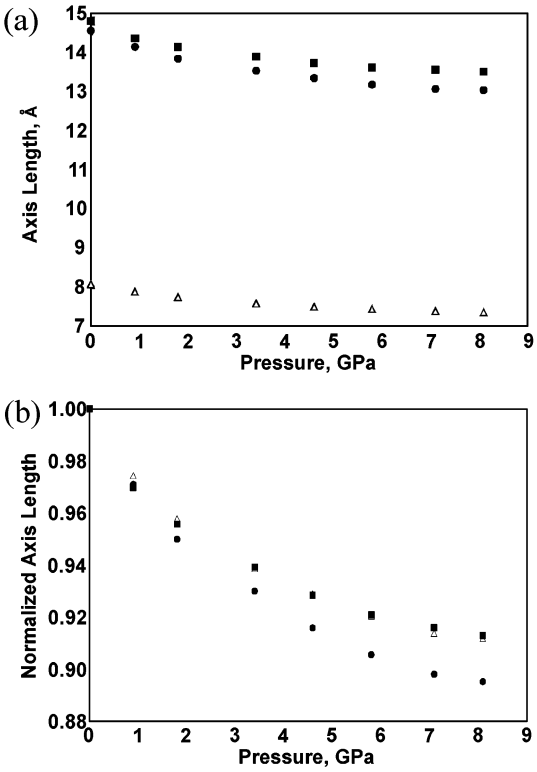


**Figure 4.** Pressure dependence of (a) unit cell dimensions and (b) normalized unit cell dimensions; $a = \triangle$, $b = \blacksquare$, $c = \bullet$. The cell dimensions are normalized to the 0.00 GPa data.

structure model. To dampen the adverse effects of any outlier reflections, the carbonyl ligands were divided into two sets on the basis of the pseudo-$D_{3h}$ symmetry (six axial carbonyls and six equatorial carbonyls), and crystallographic restraints were placed on the two sets of carbonyls. For example, at each pressure the six Ru−$C_{ax}$ distances were restrained to be approximately the same, as were the six Ru···$O_{ax}$, six Ru−$C_{eq}$, and six Ru···$O_{eq}$ distances. The underlying assumption embodied in these restraints is that all six axial carbonyls and all six equatorial carbonyls are chemically equivalent and therefore respond similarly to compression. Thus, deformation trends in the overall molecular shape can be analyzed, but potential asymmetric deformations of the Ru−C and C−O distances (or the Ru−C−O angles), which we considered unlikely, cannot be revealed in our analysis unless they become large.

A plot of the change in unit cell volume versus pressure shows no evidence for a phase transition (e.g., a discontinuity) in the 0−8.14 GPa range (Figure 3). Note that "0 GPa" refers to 1 atm ($\sim 10^5$ Pa). The plot clearly demonstrates that ruthenium carbonyl, like most molecular solids, is soft, compressing by 25% in going from atmospheric pressure to 8.14 GPa.[33] The bulk modulus of ruthenium carbonyl is 6.6 GPa. In contrast, NaCl has a value of 25 GPa, and quartz, a soft mineral, has a bulk modulus of 37 GPa. Harder materials such as ceramics have bulk moduli that range from 50 to 300 GPa, and diamond has a bulk modulus of 440 GPa. The bulk modulus can be viewed as the pressure required for a fractional change in volume. Figure 2 shows that most of the compression in ruthenium carbonyl occurs at lower pressures. The unit cell volume compresses by 21% from 0 to 4.64 GPa but by only 4% more from 4.64 to 8.14 GPa. The stiffening of the structure around 4.64 GPa is also evident in the isotropic displacement parameters, which decrease substantially between atmospheric pressure and 4.64 GPa and then change much less in the higher pressure range (Figure 3). Compression of the structure clearly results in less freedom for atomic movement. There is slight anisotropy in cell compression, with the *a*-axis, *b*-axis, and *c*-axis compressing 8.8%, 8.7%, and 10.5%, respectively, over the 8.14 GPa range (Figure 4). Importantly the pressure volume data show that the *PV* energy input is about 1760 kJ $mol^{-1}$; this far exceeds the calculated difference in energy between the anticuboctahedral structure and the smaller icosahedral, dibridged structure.[13] The fact that the structure does not shift to the smaller volume icosahedral structure suggests that there is no symmetry coordinate that links the two structures in the solid state.

The observed cell compression is due primarily to loss of the interstitial space and results in substantially decreased intermolecular distances; there is little change in actual bond lengths. For example, the Ru−Ru distances compress by an average of 2.8%, from 2.844(2) to 2.764(15) Å. (Estimated errors for averaged values respresent the standard deviation of the parameter which is related by pseudo-$D_{3h}$ symmetry, e.g., bond distance, nonbonding intramolecular contact, or bond angle. Because average intermolecular distances have no symmetry relationship, no errors are reported for these

(33) Hemley, R. J.; Dera, P. *Rev. Mineral.* **2000**, *41*, 335−419.

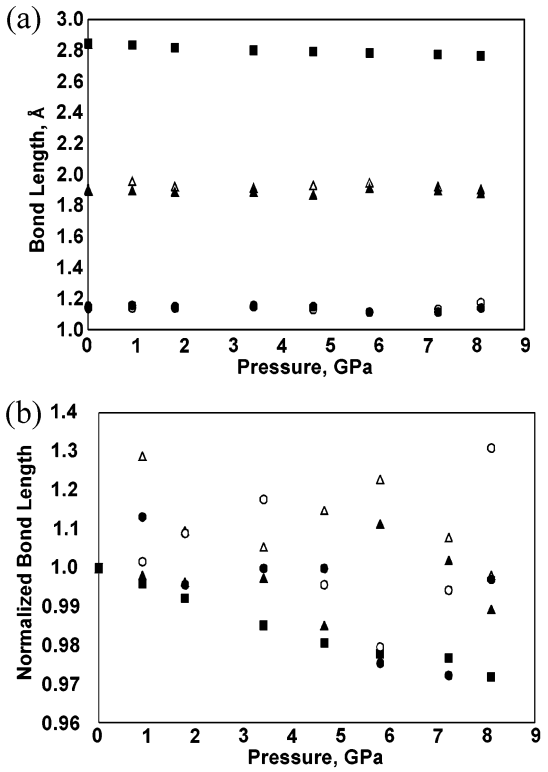


**Figure 5.** Pressure dependence of (a) average bond lengths and (b) normalized average bond lengths. Data are normalized to the 0.00 GPa data. ■ = ⟨Ru−Ru⟩, △ = ⟨Ru−$C_{ax}$⟩, ▲ = ⟨Ru−$C_{eq}$⟩, ○ = ⟨$C_{ax}$−$O_{ax}$⟩, ● = ⟨$C_{eq}$−$O_{eq}$⟩.

values.) Within the precision of the experiment, there are no changes in the Ru−C and C−O bond lengths (Figure 5). There is a slight distortion of the equatorial plane of the molecule, with the three $C_{eq}$−Ru−$C_{eq}$ angles increasing an average of 4.8° (103.5(1.1)° to 108.3(2.2)°) and the six Ru−Ru−$C_{eq}$ angles decreasing an average of 2.4° (98.3(1.8)° to 95.9(3.1)°) as pressure is increased to 8.14 GPa. These distortions are accompanied by substantial changes in intramolecular nonbonding contacts. For example, the average $O_{eq}$···$O_{eq}$ ($O_{eq}$C−Ru−Ru−$CO_{eq}$) distance compresses 10.2%, from 3.7(2) Å at ambient pressure to 3.3(5) Å at 8.14 GPa. The $O_{eq}$···$O_{eq}$ ($O_{eq}$C−Ru−$CO_{eq}$) expands 2.7%, from 4.79(4) to 4.92(9) Å (Figure 6). Although there are no significant changes in bond angles for the axial carbonyls, the decrease in the Ru−Ru distance causes a corresponding decrease in the axial nonbonding contacts as pressure increases. For example, the $O_{ax}$···$O_{ax}$ distance decreases 4.8%, from 3.03(7) to 2.90(11) Å at 8.14 GPa.

The compression in the interstitial space leads to an average decrease in intermolecular "contact" distances of 15%. In general, the shortest nonbonded distances in the compressed structure are significantly shorter than the sum of the van der Waals radii of the relevant atoms; 3.0 Å for O···O, 3.15 Å for C···O, and 3.3 Å for C···C. The average for the nearest O···O, C···O, and C···C contact distances are 2.88, 2.97, and 3.35 Å respectively, and the closest contacts are 2.54(4) Å (O···O), 2.64(6) Å (C···O), and 3.19(5) Å (C···C). The short contacts between carbonyl groups are reminiscent of the interaction observed between metal carbonyl cations and hexafluoroantimonate anions

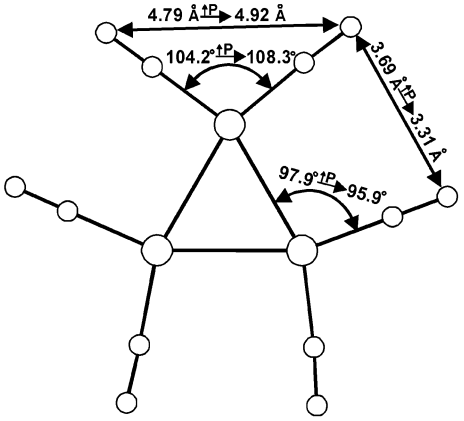


**Figure 6.** Diagram depicting the distortion of the $Ru_3(CO)_{12}$ equatorial plane with pressure.

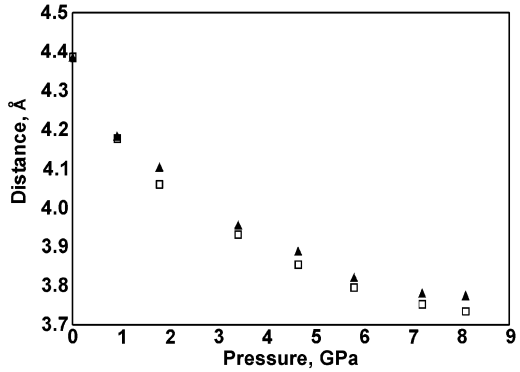


**Figure 7.** Pressure dependence of the average intermolecular Ru···O distances. □ = ⟨Ru···$O_{ax}$⟩, ▲ = ⟨Ru···$O_{eq}$⟩.

where C···F distances can be as short as 2.59 Å.[34] For example, $[Ir(CO)_6][SbF_6]_3$·4HF, which resembles $Ru_3(CO)_{12}$ with its coordinatively saturated octahedral metal center, has C···F contacts of 2.65−2.99 Å.[34]

Intermolecular compression was further analyzed by separating contacts into intermolecular Ru···O, O···O, C···O, and C···C contact distances and then further separating and averaging the ax···ax, ax···eq, and eq···eq distances (Figures 7−9). Individual O···O, O···C, and C···C contact distances between clusters decreased by as much as 28%. At each pressure, the Ru···$O_{ax}$ and Ru···$O_{eq}$ distances are essentially identical (Figure 7), which raises the question of whether this is a simple coincidence or whether Ru···O repulsions are a more significant factor in determining crystal packing than one otherwise would have anticipated. There is a slight anisotropy in the O···O and O···C compression (Figure 8a,b) with the ax···eq contact distances exhibiting the greatest compression. The average $O_{ax}$···$O_{eq}$ distance decreases 0.53 Å from 3.39 Å (0.00 GPa) to 2.86 Å (8.14 GPa), and the average $O_{eq}$···$C_{ax}$ distance decreases 0.61 Å, from 3.50 Å to 2.89 Å. Although the average $C_{ax}$···$C_{ax}$, $C_{ax}$···$C_{eq}$, and $C_{eq}$···$C_{eq}$ distances differ by 0.1−0.2 Å at each pressure, like the Ru···O distances, the overall compression is isotropic (Figure 8c). At 0.00 GPa, the average C···C contact distances range from 3.87 Å ($C_{ax}$···$C_{eq}$) to 3.71 Å ($C_{ax}$···$C_{ax}$). At 8.14 GPa, the respective distances are 3.43 and 3.32 Å.

(34) Willner, H.; Aubke, F. *Organometallics* **2003**, *22*, 3612−3633.

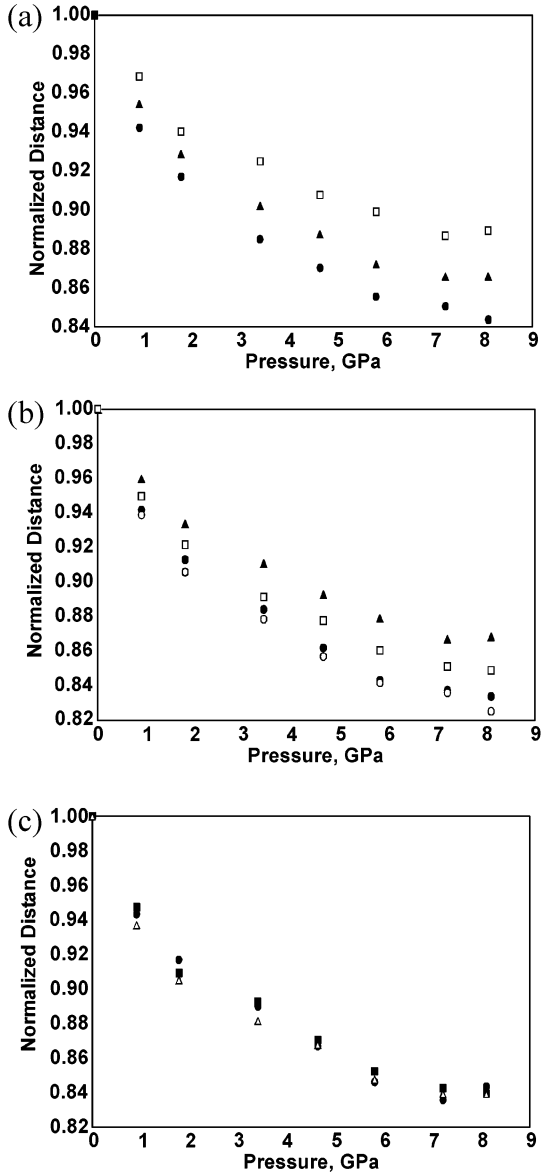


**Figure 8.** Pressure dependence of average intermolecular contact distances normalized to the 0.00 GPa data. (a) Normalized ⟨O···O⟩ distances: □ = ⟨$O_{ax}$···$O_{ax}$⟩, ▲ = ⟨$O_{eq}$···$O_{eq}$⟩, ● = ⟨$O_{ax}$···$O_{eq}$⟩. (b) Normalized ⟨O···C⟩ distances: □ = ⟨$O_{ax}$···$C_{ax}$⟩, ▲ = ⟨$O_{eq}$···$C_{eq}$⟩, ● = ⟨$O_{ax}$···$C_{eq}$⟩, ○ = ⟨$O_{eq}$···$C_{ax}$⟩. (c) Normalized ⟨C···C⟩ distances: □ = ⟨$C_{ax}$···$C_{ax}$⟩, ▲ = ⟨$C_{eq}$···$C_{eq}$⟩, ● = ⟨$C_{ax}$···$C_{eq}$⟩.

Visually, the most significant difference between the low-pressure and high-pressure structures is the interleaving of the carbonyl groups from one ruthenium cluster to a neighboring cluster. In the low-pressure structures, intermolecular distances show a clear trend with O···O < O···C < C···C. As pressure is increased, interleaving of neighboring carbonyls increases, and the carbonyl oxygens get closer to being equidistant from the C and O of the neighboring carbonyls (Figure 9).

There have been extensive vibrational spectroscopy studies on trinuclear ruthenium and osmium carbonyls, $M_3(CO)_{12}$, M = Ru, Os, at ambient conditions.[35−39] The ruthenium and osmium clusters have $D_{3h}$ symmetry which leads to 34 Raman-active modes and 21 infrared-active fundamentals. Vibrational spectra of metal carbonyls can be divided into 3 regions: (1) a low-frequency region (<300 $cm^{-1}$) resulting from Ru−Ru stretching and Ru−C deformation, (2) an intermediate region (350−650 $cm^{-1}$) corresponding to Ru−C stretching and carbonyl bending vibrations, and (3) the carbonyl stretching region at high frequency (1950−2190 $cm^{-1}$).

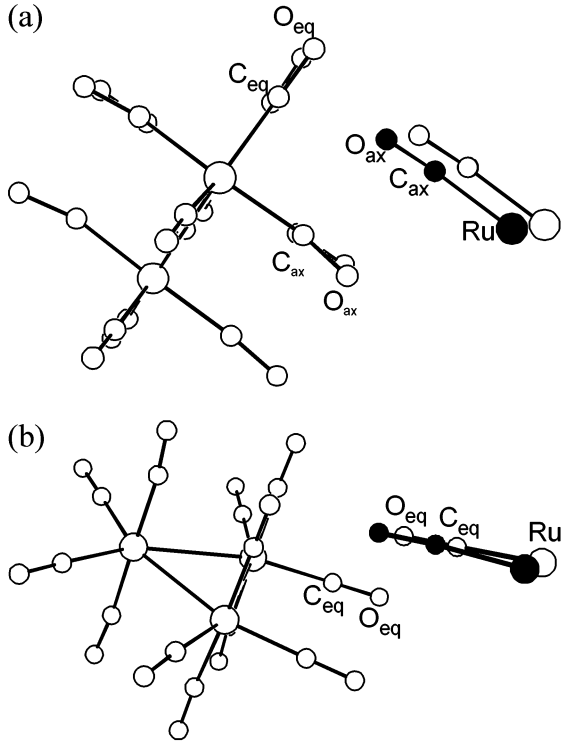


**Figure 9.** Schematic diagram showing the $Ru_3(CO)_{12}$ molecule at 0.00 GPa and selected atoms from a neighboring molecule at 1 atm (○) and 8.10 GPa (●). (a) View depicting ax···ax and ax···eq interactions. (b) View depicting eq···eq interactions.

We report here variable pressure Raman studies of the 3 spectral regions and variable pressure IR studies of the carbonyl region. The Raman spectra for $Ru_3(CO)_{12}$ as a function of pressure are shown in Figure 10a, and IR spectra in the carbonyl region at ambient pressure inside and outside the moissanite anvil cell are shown in Figure 10b. All three spectral regions show changes in peak shape and an increase in number of observed bands with increased pressure. For example, 12 Raman active modes are predicted for the low frequency region. At ambient pressure, only 2 prominent peaks are observed. With increasing pressure, the relative intensities of these two peaks switch, the line widths broaden, and an asymmetric band shape with fine structure appears. These changes are all indicative of stronger interactions among the vibrational groups as pressure is increased. Similarly, for the intermediate frequencies, 16 bands are predicted, but only 3 are observed at ambient pressure; however, up to 7 bands are resolvable at intermediate pressures.

(35) Quicksall, C. O.; Spiro, T. G. *Inorg. Chem.* **1968**, *7*, 2365.
(36) Kettle, S. F. A.; Stanghellini, P. L. *Inorg. Chem.* **1979**, *18*, 2749.
(37) Battiston, G. A.; Bor, G.; Dietler, U. K.; Kettle, S. F. A.; Rosseti, R.; Sbrignadello, G.; Stanghellini, P. L. *Inorg. Chem.* **1980**, *19*, 1961−1973.
(38) Adams, D. M.; Taylor, I. D. *J. Chem. Soc., Faraday Trans. 2* **1982**, *78*, 1561−1571.
(39) Butler, I. S.; Xu, Z. H.; Darensbourg, D. J.; Pala, M. **1987**, *18*(5), 357−363.

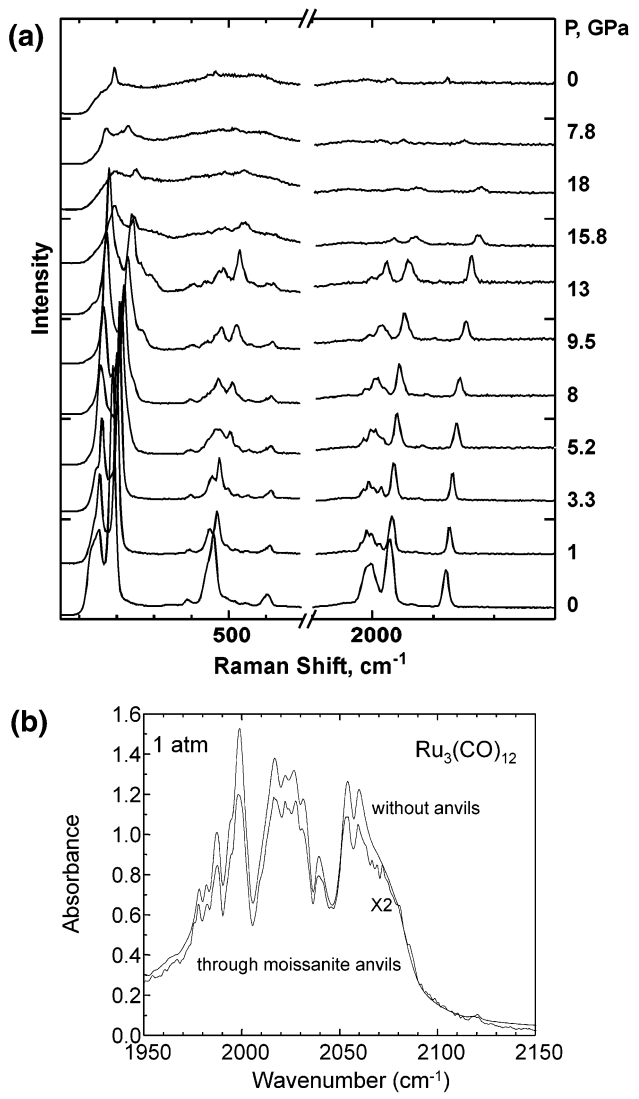


**Figure 10.** (a) Representative Raman spectra as a function of pressure. Spectra are collected on compression from ambient to 18 GPa and then on decompression to ambient via 7.8 GPa (top two spectra). (b) Representative infrared spectrum in the moissonite anvil cell in the carbonyl region.

Six Raman-active fundamentals are predicted in the high-frequency region, but these fundamentals can further split due to stretch−stretch interactions across the cluster. Ambient pressure splitting analysis indicates interactions among equatorial carbonyls yields vibrations around 1989−2011 $cm^{-1}$ while the axial carbonyls give vibrations in the region 2028−2127 $cm^{-1}$.[35] At ambient pressure, only three prominent peaks are observed in the DAC. The band at 1995 $cm^{-1}$ is assigned to the equatorial carbonyls, and the peaks at 2027 and 2120 $cm^{-1}$ are assigned to axial CO stretching modes. These observations are consistent with previous Raman measurements at ambient conditions where the three strongest bands occur at 1994, 2028, and 2127 $cm^{-1}$, respectively.[34] As with the lower frequency regions, higher pressures increase stretch−stretch interactions and allow more Raman bands to be resolved. Compression to just 1 GPa results in the resolution of seven modes. Peak broadening is observed above 10 GPa, and beyond 15.8 GPa, only three modes of relatively weak intensity are observed. In the infrared

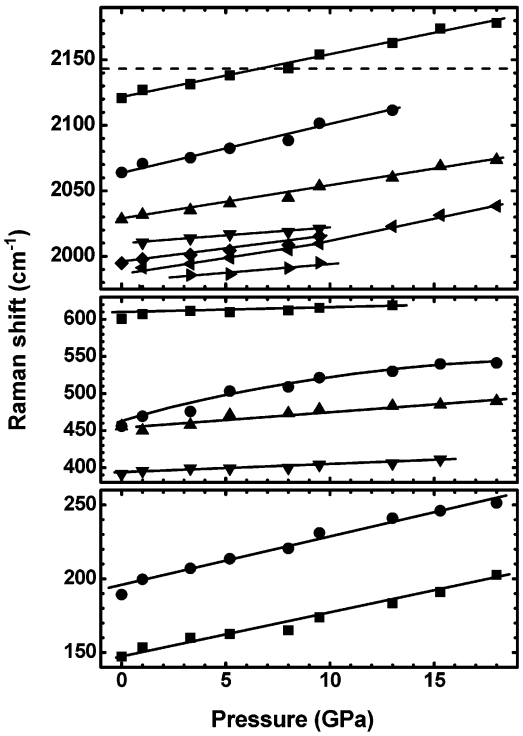


**Figure 11.** Plot of observed Raman frequencies as a function of pressure for $Ru_3(CO)_{12}$ shown in three panels, from bottom to top, corresponding to Ru−Ru stretching, Ru−C deformation, and C−O stretching, respectively. Different symbols denote different vibrational modes. The horizontal dashed line at 2143 $cm^{-1}$ denotes the vibrational frequency of free CO.

spectrum, a total of 17 modes are observed at ambient pressure, and their frequencies agree well with previously reported data.[37]

When the pressure is elevated to 18 GPa, the highest pressure of current study, the Raman sample irreversibly transforms from semitransparent to totally dark, and a nearly featureless Raman pattern is observed. In contrast, the infrared spectrum obtained upon quenching the high-pressure sample is similar to the original ambient temperature spectrum with the exception of some differences in relative intensities, suggesting that some residual strain may linger. On the basis of these observations, we conclude that the ruthenium−carbonyl cluster is destroyed by the Raman laser under high pressure.

The Raman and IR frequencies of individual deconvoluted bands as a function of pressure are plotted in Figures 11 and 12. All the bands move to higher frequency, which is consistent with previous high-pressure experimental work[22,40] and theoretical models.[41] It is useful to examine possible correlations between the measured changes in bond lengths and the frequency shifts (or force constant changes).[41] The structure refinements to 8.14 GPa reveal no significant changes in Ru−C and C−O bond lengths but a 2.8% decrease in the Ru−Ru distance over the measured pressure range (Figure 5), indicating that the correlation between bond lengths and force constants is weak. Nonetheless, there seems to be a qualitative correlation between the bond length

(40) Adams, D. M.; Ruff, P. W.; Russell, D. R. *Journal of the Chemical Society-Faraday Transactions* **1991**, *87*(12), 1831−1836.
(41) LeSar, R.; Herschbach, D. R. *J. Phys. Chem.* **1981**, *85*, 2798−2804.

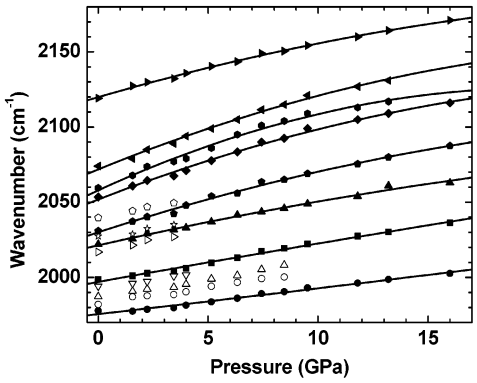


**Figure 12.** Plot of wavenumber vs pressure from the high-pressure infrared spectra in the carbonyl region. The solid lines are the linear best fits to those peaks observable above 9 GPa (solid symbols) with $\nu = \nu_0 + (a \times P) + (b \times P^2)$. The open symbols represent the shoulders or peaks with weak intensities. A table of frequencies and values for *a* and *b* is included with the Supporting Information.

changes and frequency shifts. For example, the pressure derivatives of the Raman shifts in the Ru−Ru, Ru−C, and C−O stretching regions range from 3.9 to 5.2 $cm^{-1}$/GPa, from 1.3 to 1.9 $cm^{-1}$/GPa, and from 2.5 to 3.4 $cm^{-1}$/GPa, respectively, in accord with the observation that the largest change occurs in the Ru−Ru distance. A full normal coordinate analysis is required to provide additional insight.

The vibrational frequency shifts with pressure (Figure 11) show slight changes in slope in the 5−10 GPa range. Similar observations for $Mn_2(CO)_{10}$ and $Re_2(CO)_{10}$ were ascribed to phase changes.[22] However, the diffraction data obtained here for $Ru_3(CO)_{12}$ show no evidence for major structural changes from 0 to 8.14 GPa (Figure 3). Additional experimental data in related systems is clearly needed to understand this behavior, and work toward that end is underway in our laboratories.

**Acknowledgment.** Virginia Tech provided funds for the purchase of the Oxford Diffraction Xcalibur diffractometer. The authors acknowledge with gratitude the financial support for this work derived from NSF Grant EAR-0105864. Ruby pressure measurements were conducted with the Raman system in the Vibrational Spectroscopy Laboratory in the Department of GeoSciences at Virginia Tech. We thank Professors Paul A. Deck, Nancy Ross, and T. Daniel Crawford for helpful discussions.

**Supporting Information Available:** Crystallographic data in CIF format and additional IR data in PDF format. This material is available free of charge via the Internet at http://pubs.acs.org.

IC049617Y